PERGAMON

Solid State Communications 115 (2000) 29–34

solid state communications

www.elsevier.com/locate/ssc

Phase-coherent conduction in mesoscopic normal-metal/superconductor hybrid junctions

N. Kim[a], H.-J. Lee[a,*], J.-J. Kim[b], J.-O. Lee[b], J.W. Park[c], K.-H. Yoo[c], S. Lee[d], K.W. Park[d]

[a]*Department of Physics, Pohang University of Science and Technology, Pohang 790-784, South Korea*
[b]*Department of Physics, Chonbuk National University, Chonju 561-756, South Korea*
[c]*Electricity Group, Korea Research Institute of Standards and Science, Taejon 305-600, South Korea*
[d]*Telecommunication Basic Research Laboratory, Electronics and Telecommunications Research Institute, Taejon 305-350, South Korea*

Received 13 December 1999; accepted 17 March 2000 by T. Tsuzuki

Abstract

In this paper we report about the transport properties of mesoscopic normal-metal/superconductor (NS) hybrid systems with two different junction layouts. One is a junction fabricated by overlaying S on N wire and the other with S sandwiched between two N wires, forming an NSN structure. At zero bias all the junctions exhibited a sharp decrease of dV/dI, which is believed to arise from the interference between the disorder-scattered and the Andreev-reflected quasiparticles. A small magnetic field corresponding to one flux quantum through the normal metal region, applied in parallel with the NS junction, easily suppressed the anomalous zero-bias conductance enhancement for the sandwich-junction sample. This high sensitivity to a small magnetic field observed in our systems of mesoscopic NS junctions in a diffusive-transport regime directly confirms the electron–hole-interference origin of the zero-bias anomaly. © 2000 Published by Elsevier Science Ltd. All rights reserved.

Keywords: Heterojunctions; A. Nanostructures; A. Surfaces and interfaces; D. Electronic transport

1. Introduction

The recent development of microfabrication technology enables experimental access to the proximity effect in various mesoscopic normal-metal/superconductor (NS) or semiconductor/superconductor (SmS) hybrid junctions [1]. An incident electron from the normal-metal side onto the NS interface is reflected back as a hole, while a condensed superconducting pair propagates through the superconductor. In this Andreev scattering process [2] occurring at the interface of NS or SmS junctions the phase coherence between the conjugate pair of an electron and a hole, which leads to an enhancement of the conductance, is the key element of interest. For a normal-metal electrode in a ballistic-transport regime in contact with a superconductor, it is well known that the conductance follows the Blonder–Tinkham–Klapwijk (BTK) theory [3]. For transparent hybrid junctions the Andreev reflection gives an enhanced zero-bias conductance, while in the presence of a finite scattering barrier at the interface, the Andreev reflection probability is reduced along with the reduction of the conductance.

For a diffusive system of NS or SmS junctions [4,5], however, electrons and holes are scattered by the existing disorder in the N or Sm electrode near the interface and the conducting properties deviate from the BTK prediction. For instance, a zero-bias enhancement of the conductance was observed in the diffusive SmS junctions [5] with a finite scattering barrier at the interface. The phenomenon, referred to as the zero-bias anomaly (ZBA), is in apparent contradiction to the conductance reduction predicted by the BTK theory. The ZBA is believed to arise from the disorder-enhanced multiple scattering of electrons and holes near the interface and the resulting interference between these conjugate particles. The phenomena have been treated theoretically using a quasiclassical theory [6–10] and a scattering matrix approach [10–14]. In addition to the ZBA, the interference pattern of conductance in diffusive NS junctions [15,16] modulated by the external magnetic fields or currents and the reentrance of conductance in NS proximity

* Corresponding author. Tel.: +82-562-279-2072; fax: +82-562-279-3099.

E-mail address: hjlee@postech.ac.kr (H.-J. Lee).

PII: S0038-1098(00)00120-4

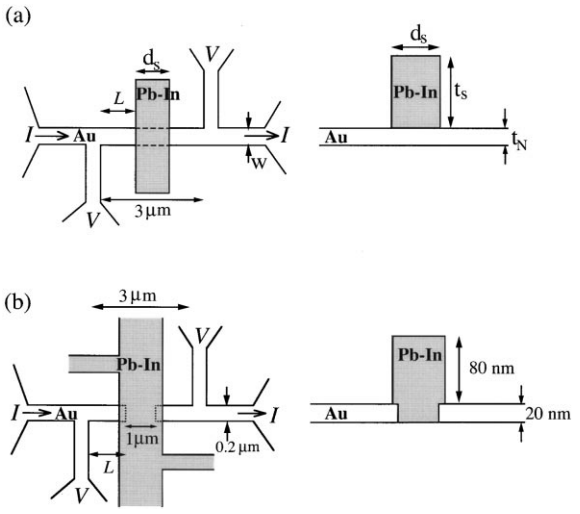

Fig. 1. Schematic diagram of the sample geometry for Samples OL1 and OL2 (a), and Sample SW1 (b). (a) w and t_N are the width and the thickness of the normal metal, respectively. d_s and t_s are the width and the thickness of the superconducting island, respectively. $w = 0.2$ μm, $t_N = 25$ nm, $d_s = 0.3$ μm, and $t_s = 150$ nm for OL1, and $w = 0.3$ μm, $t_N = 30$ *nm*, $d_s = 1$ μm, and $t_s = 100$ nm for OL2. (b) $w = 0.2$ μm, $t_N = 30$ nm, $d_s = 1 - 1.4$ μm, and $t_s = 95$ nm for SW1.

junctions [17] have been also explained well by the quasiclassical theory. From the theoretical points of view, most of the proximity effects in diffusive NS junctions mentioned above seem to be explained satisfactorily by the existing theories. However, as for the magnetic field dependence of the ZBA, two contradictory experimental observations have been reported, which necessitate further studies. The conductance of SmS junctions [5] was highly sensitive to an external magnetic field as low as a few tens of mT, when applied in parallel with the junction area. On the other hand, the conductance of NS junctions [4] turned out to be robust to a magnetic field of as high as a few T, when applied again in parallel with the junction. The latter result is contradictory to the expected field effect on the phase coherence between conjugate particles, because the conductance variation due to phase coherence should be sensitive to the magnetic field applied in parallel with the junction cross-section [11,14].

Since the interference between electrons and holes plays such an important role in diffusive NS junctions the conductance of junctions, especially in an external magnetic field, sensitively depends on the details of their geometry [6,7]. In this study, to clarify the role of phase coherence between conjugate particles in the ZBA phenomena, we examined the sensitivity of the conductance both in the absence and in the presence of a magnetic field to the junction geometry using two types of junctions. The "overlay" junction was fabricated by depositing a superconducting island (S) onto a normal metal (N) wire as shown in Fig. 1(a). The "sandwich" junction was fabricated by placing a superconducting island between the normal electrodes (see Fig. 1(b)). For all the samples, a highly nonlinear bias dependence of dV/dI developed, including the ZBA and a kink in the differential conductance above the gap ("above-gap anomaly") appeared, but everything disappeared above the critical temperature of the superconducting island. Some distinctive features were observed for the two different-geometry samples. First, the probability of the Andreev reflection was enhanced in the overlay junctions compared with the sandwich junctions, presumably because particles in the overlay junctions underwent more multiple scattering at the NS interface, thus enhancing the Andreev scattering probability. Second, when k_BT or eV was larger than the Thouless energy E_c, the conductance was observed to follow the relation $1/\sqrt{k_BT + eV}$ in overlay NSN junctions, which is in agreement with the prediction of the quasiclassical theory [9,10]. It implies that the normal-metal coherence length $\xi_N(k_BT, eV)$ shrinks as $1/\sqrt{k_BT + eV}$, with increasing temperatures or the bias voltages. However, such conductance behavior was not present in the sandwich NSN junction, presumably because the voltage difference across the NS interface in the sandwich-junction sample was added to the proximity effect. Finally, we observed a sharp drop of magnetoresistance for a field $H < H^*$ far below the critical field H_{c2}, which we attributed to the field-induced destruction of the phase coherence between the electron–hole pairs. The ZBA observed in the sandwich-junction sample turned out to be very sensitive to a magnetic field as low as a few hundreds of gauss as applied in parallel with the interface. The critical field which destroyed the ZBA corresponded to one flux quantum($= h/e$) through the normal-metal area, in agreement with the theoretical prediction based on a scattering-matrix theory [14]. On the other hand, the ZBA of the overlay junction was robust to a magnetic field applied perpendicular to the interface. These behaviors confirmed that the ZBA was caused by the phase coherence between the multiple scattered conjugate particle pairs near the interface.

2. Experiment

The transport properties of the system can be sensitive to the configuration of disorder and the shape of the NS interface [6,7]. Using e-beam lithography and the conventional lift-off technique, we fabricated three mesoscopic samples consisting of NSN junction structure as shown in Fig. 1. Two are overlay junctions (Samples OL1 and OL2) and the other is a sandwich junction (Sample SW1). For an N electrode, high-purity (99.9999%) Au was thermally deposited onto a Si wafer, which was pre-coated with a thin (1 nm in thickness) Ti film to enhance the adhesion of the Au film to the substrate. The Ti film was thin enough, so as not to affect the transport properties of the samples to be made on top of it. The line width and the thickness of Au

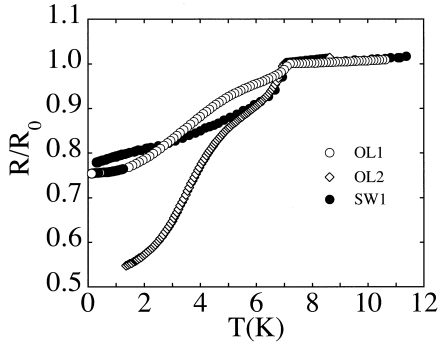

Fig. 2. Normalized resistance R/R_0 vs T for the samples as taken in a sample current in the range 1–2 μA. The normal-state resistance R_0 is defined as the one at the critical temperature of the Pb island, $T_{c,Pb} = 7.0$–7.2 K. The values of R_0 are 32.4, 15.5, and 8.1 Ω, for Samples OL1, OL2, and SW1, respectively.

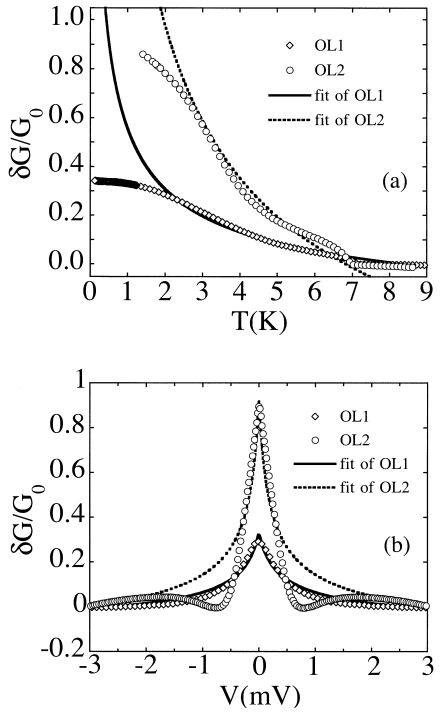

Fig. 3. (a) Conductance variation $\delta G(\equiv (G - G_0)/(G_0))$ as a function of temperature for overlay-junction samples, where $G_0 \equiv R_0^{-1}$. The solid and dotted lines are fits to the relation $a((E_c/k_BT)^{1/2} - b)$, with the best fit value for the Thouless energy given as $E_c = 5.2$ μeV for both samples. The fit constants a and b are $a = 3.3$ and $b = 0.28$ for OL1 and $a = 11.7$ and $b = 1.1$ for OL2. (b) The conductance variation δG as a function of bias voltage V for the overlay samples OL1 at $T = 1.5$ K and OL2 at $T = 0.30$ K. The solid and dotted lines are fits to the relation $a'((E_c/eV + \alpha)^{1/2} - b')$, with the best-fit values of $a' = 2.9$, $b' = 0.12$, and $\alpha = 0.20$ meV for OL1, and $a' = 5.0$, $b' = 0.20$, and $\alpha = 0.10$ meV for OL2.

were 200–300 nm and 25–30 nm, respectively. We then overlaid (sandwiched) an S electrode on the N electrode (between the two N electrodes) by depositing and lifting off the Pb film for the overlay junctions (sandwich junction). About three weight percent of In was added to Pb to enhance the film homogeneity. The distance between the voltage probes was 3 μm for all three samples.

The length of the superconducting islands for Samples OL1 and OL2 was 0.3 and 1.0 μm, respectively. To compare the effect of the junction geometry on the proximity effect between the two types of junctions, the length of the sandwiched superconducting island in SW1 was fabricated to be the same as that of the overlayed superconducting island in OL2, i.e. 1.0 μm. Details of the geometry of each sample are described in the captions. The geometry of Sample SW1 is designed to measure the transport characteristics directly through the S electrode in NSN junctions. The typical resistivity of Au wires was 5.4 μΩ cm corresponding to the diffusivity $D \approx 70$–80 cm^2/s. Using the formula given by the authors [18] we can estimate from the resistivity that the phase coherence length l_ϕ is 1.6 μm at $T = 1$ K. Thus, our samples were in a phase-coherent state in the temperature range below 1 K. All the transport data such as $R(T)$ and dV/dI vs V were measured using the conventional lock-in technique in the low frequency range of 30–40 Hz.

3. Results and discussion

3.1. R(T) characteristics

Fig. 2 shows the temperature dependencies of the resistance $R(T)$ of the three samples used: Samples OL1 (open circle), OL2 (open diamond), and SW1 (solid circle). The resistance of each sample shows a sudden drop at the superconducting transition temperature of the Pb islands $T_{c,Pb}$ (≃7.0–7.2 K). Below $T_{c,Pb}$, the $R(T)$ of Samples OL1 and OL2 are qualitatively similar. With lowering of temperatures, the $R(T)$ of the two samples show a slower decrease, but followed by a faster reduction with a long finite-resistance tail at the low-temperature limit. On the other hand, the $R(T)$ curve of Sample SW1 shows a downturn curvature in the whole temperature range below $T_{c,Pb}$. The data for Samples OL1 and OL2 are replotted in Fig. 3(a) in terms of the relative conductance variation $(\delta G(T))/(G_0) \equiv (G(T) - G_0)/(G_0)$, where the reference conductance $G_0(= R_0^{-1})$ is the value at $T_{c,Pb}$. As illustrated by the dotted and the solid lines in the figure, in the high-temperature range ($T > 3$ K), $\delta G/G_0$ follows the temperature dependence of $a\sqrt{(E_c)/(k_BT)} - b$, well, where $E_c = \hbar D/L^2$ is the Thouless energy, a and b are constants, and L and D are the length and the diffusivity of the normal-metal electrodes of both samples, respectively. Here, the parameter b is introduced to set $\delta G/G_0$ at $T_{c,Pb}$ to be zero. Thus the exact value of b has little physical significance. Here, $E_c = 5.2$ μeV(≈ 60 mK),

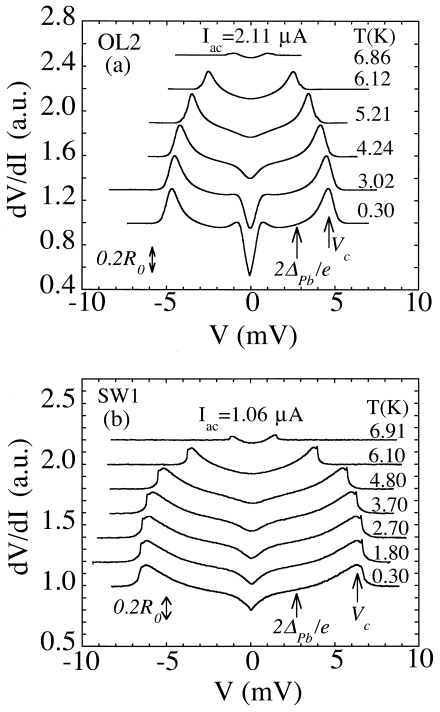

Fig. 4. Normalized dynamic resistance dV/dI vs V at various temperatures for samples OL2 (a) and SW1 (b). The curves are normalized by the value at T_c and shifted vertically for clarity.

assuming $D = 80$ cm^2/s and $L = 1$ μm. The best fit values of the constant a are 3.3 and 11.7 for Samples OL1 and OL2, respectively, which are much larger than the value predicted by the quasiclassical theory [9]. According to Golubov [9] $\delta G/G_0$ in the limit $k_B T \gg E_c$ is predicted to follow the relation $0.42\sqrt{(E_c)/(k_B T)}$. The general $1/\sqrt{T}$ dependence follows from the classical proximity effect. With the lowering of temperature, the superconducting pair penetration expands due to the proximity effect into the normal electrode up to the thermal coherence length $\xi_N(T) = \sqrt{(\hbar D)/(2\pi k_B T)}$, along with the reduction of the resistance, in proportion, by $R_0 \times \xi_N(T)/L$. $\delta G/G_0$ in Fig. 3(a) deviates from the $1/\sqrt{T}$ dependence at the low-temperature limit. We believe that the deviation results from the energy dependence of the spectral conductance $g(\epsilon)$ [19]. In this case, one must integrate $g(\epsilon)$ over all available energies to calculate the conductance at the low-temperature limit. The $1/\sqrt{T}$ dependence of $\delta G(T)$ is observed only in Samples OL1 and OL2, where in this overlay structure the tunneling resistance across NS interfaces is not included in the resistance data. In contrast, $\delta G(T)$ of the sandwich-junction sample, SW1, does include the interfacial tunneling resistance, which presumably washes out the $1/\sqrt{T}$ dependence of $\delta G(T)$.

3.2. d$V(T)$/dI vs V characteristics

Fig. 4 shows the measured dynamic resistance d$V(T)$/dI at various temperatures for Samples OL2 and SW1. The temperature dependence of dV/dI for Sample OL1 (not shown) is similar to that of Sample OL2. All the samples commonly show zero-bias resistance dips with onset biases below double the Pb gap voltage ($2\Delta_{Pb}/e = 2.7$ meV). At bias voltages higher than $2\Delta_{Pb}/e$ the resistance peaks above the normal-state resistance, i.e. the above-gap anomaly, develop at a critical voltage V_c as shown in the figure. With increasing temperatures both the zero-bias dip and the above-gap anomaly get smeared and vanish upon approaching $T_{c,Pb}$, with the magnitude of V_c decreasing continuously. All the nonlinearity in dV/dI disappears above $T_{c,Pb}$.

The appearance of the zero-bias dip in dV/dI below the superconducting gap voltage and the sharpness of its shape is in contradiction to the prediction of the BTK theory. It is now generally accepted [6–13] that the ZBA is due to an interplay between the Andreev reflection at the NS interface and the normal electron scattering due to disorder in the N electrodes. According to the quasiclassical theory [9,10] the zero-bias dip or the conductance enhancement $\delta G/G_0$ should follow a $1/\sqrt{V}$ bias dependence for the $eV \gg E_c$ limit. In a diffusive NS junction, the momentum mismatch of electrons and holes increases with increase in the bias voltage, along with the decrease in the phase-coherent Andreev reflection probability. It would result in a conductance suppression [11] with increasing V. In fact, Fig. 3(b) shows that the conductance decreases qualitatively as $1/\sqrt{eV + \alpha}$, where the parameter α is introduced to take into account the thermal phase-breaking effects occurring in normal metals. The values turn out to be about 0.20 meV (≃2.3 K) and 0.10 meV (≃1.2 K) for Samples OL1 and OL2, respectively, which are somewhat higher than but quite close to the corresponding measurement temperatures 1.5 and 0.30 K, respectively.

In Fig. 5 we plotted the excess current defined as $I_{exc}(V) = I(V) - V/R_0$ (R_0 is the normal-state resistance) as a function of bias voltages normalized by the gap voltage. The existence of the excess current indicates that the zero-bias dip of the differential resistance as shown in Fig. 4 is due to the Andreev reflection effect. I_{exc} increases for a bias below the gap voltage, reaches a maximum and then decreases to a constant value around the critical bias voltage V_c. Similar $I_{exc}(V)$ characteristics were also observed in SSmS structures [20]. The decrease of the excess current for $eV > 2\Delta_0$, however, is not clear. I_{exc} is larger for Sample OL2 than for Sample OL1. According to the BTK theory the Andreev-reflection-induced I_{exc} is sensitive to the barrier potential at the NS interface due to the existence of impurities and the Fermi-surface mismatch between N and S: the excess current decreases monotonically as the strength of the scattering barrier increases. $I_{exc}(V)$ in Fig. 5 indicates that the Andreev reflection probability in Sample OL2 is higher than in Sample OL1. The effect is believed to arise because the length of the S island overlaid on N is significantly larger in OL2, which apparently enhances the

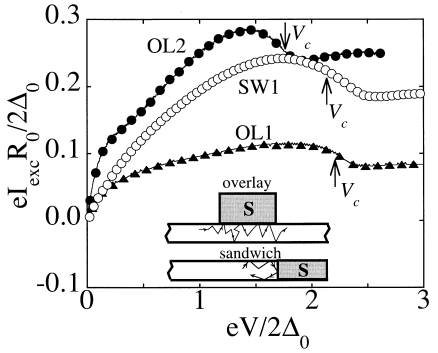

Fig. 5. Normalized excess current as a function of normalized bias voltage for the samples at temperatures 1.5 K (for OL1) and 0.30 K (for OL2 and SW1). The excess currents I_{exc} are obtained from corresponding current–voltage curves and we use $\Delta_{Pb} = 1.35$ meV as the gap energy for the Pb island. The arrows indicate the critical bias voltage V_c, as defined in Fig. 4, for each sample.

Andreev reflection probability at the NS interface (see the inset of Fig. 5).

The magnitude of I_{exc} for Sample SW1 is smaller than Sample OL2, although the length between the voltage probes and the length d_s of the superconducting island for both samples are not significantly different. This can be explained by the difference in the junction geometries between the two samples. As can be expected from the inset of Fig. 5 more multiple reflection of particles is possible along the NS interface of Sample OL2 than Sample SW1, which gives the higher probability of the Andreev reflection in Sample OL2. This gives additional confirmation that the ZBA arises from the disorder-enhanced Andreev reflection near the interface.

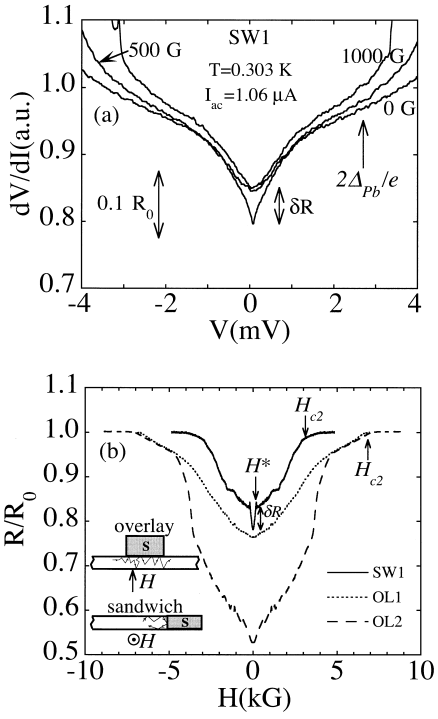

Fig. 6. (a) Normalized dV/dI vs V for Sample SW1 at $T = 0.30$ K for biases far below V_c (the same quantity as defined in Fig. 4) in various magnetic fields. The probing sample current is 1.06 μA. (b) Normalized magnetoresistance at $T = 0.078$ K (for OL1) and $T = 0.30$ K (for OL2 and SW1). H^* denotes the characteristic field where a rapid resistance change occurs far below the critical field H_{c2} of the superconducting Pb island. $\delta R \equiv R(H = H^*) - R(H = 0)$.

3.3. dV/dI *vs* V *in magnetic fields*

Since a magnetic field causes variations in the phases of both electrons and holes it would suppress the disorder-induced Andreev reflection probability [11,14]. Thus, application of magnetic fields is expected to destroy the sharp zero-bias dip in the dynamical resistance. Fig. 6(a) shows the dV/dI data around zero bias at 0.30 K for Sample SW1, when a relatively low magnetic field is applied in parallel with the NS interface (see the inset of Fig. 6(b)). As the magnetic field is increased the zero-bias resistance dip smears out rapidly, even in the presence of a magnetic field as low as $H = 500$ G (Fig. 6(a)).

The magnetoresistance (MR) data (Fig. 6(b)) for Sample SW1 (solid line) at $T = 0.30$ K in the zero-bias limit also provides a clue to the mechanism of the magnetic-field effect on the zero-bias dip. The MR data show a feature of double resistance transition, one of which occurs at the magnetic field denoted as $H^*(\approx 200$ G) and the other at the critical field $H_{c2}(\approx 3$ kG). In Ref. [14], the authors predicted that the width of the MR dip due to the interference effects between the electrons and the Andreev-reflected holes is of an order $H_c = h/eLW$, where h/e corresponds to the one flux quantum, L and W are the length and the width of the normal-metal electrode, respectively, along the directions perpendicular to an applied magnetic field. H_c turns out to be ~200 G for Sample SW1, which corresponds to the one flux quantum through the normal-metal region between a voltage lead and the superconductor. The agreement of the value of H^* with that of H_c supports our previous arguments that the sharp zero-bias resistance dip originates from the interference between the disorder-scattered and the Andreev-reflected conjugate particle pairs at the NS interface. Such a sharp increase of MR at H^* as in Sample SW1 is not observed in Samples OL1 (dotted line) and OL2 (dashed line), where a magnetic field was applied in perpendicular to the plane of NS junctions (see the inset of Fig. 6(b)). In the overlay-junction specimens the trajectory of the electron paths tends to form more in parallel with the field direction than in the sandwich-junction specimen, where the plane of the closed paths are formed in perpendicular to the field direction. The high sensitivity of the resistance to a magnetic field, in parallel with the NS junctions also supports our arguments. However, the magnitude of $\delta R/R^2$, the zero-bias conductance variation due to magnetic

fields, is approximately $150e^2/h$, which is about two orders of magnitude larger than the theoretical prediction [14]. In Ref. [5], an even larger variation of the magnetoresistance is reported.

The authors of Ref. [4] also observed a rapid increase of resistance in a field below a characteristic field denoted as H' in NS junctions, which is smaller than H_{c2}. They proposed that H' corresponded to the field at which the superconducting electrode became gapless while remaining superconducting based on the fact that the above-gap anomaly disappeared in the presence of magnetic fields higher than H'. However, these arguments cannot be applied to our data because, contrary to their case, the above-gap anomaly still existed (not shown) in the presence of magnetic fields between H^* and H_{c2}.

3.4. V_c vs T

For all the samples the critical voltage V_c is more than twice as large as the superconducting gap voltage. Surprisingly, their temperature dependence follows the BCS temperature dependence of the gap [21] well (not shown), regardless of the difference in the junction geometry. A similar temperature dependence of V_c has been observed previously in SmS- and NS-junction systems [4,20]. The critical current J_c corresponding to the bias voltage V_c for all the samples is $3–4 \times 10^6$ A/cm^2, which is at least an order of magnitude smaller than that of the superconducting wire [22]. However, as pointed out by the authors of Ref. [4], it is high enough to affect the local contact resistance. This reasoning agrees with the fact that I_{exc} or the Andreev reflection probability decreases around V_c as shown in Fig. 5. We suppose that the injected current density J_c increases the local resistance of an NS junction due to local suppression of superconductivity, resulting in the decrease of the Andreev reflection probability. But further study is necessary to clarify why the critical current density in NS junctions is proportional to the superconducting gap.

4. Summary

We have observed the ZBA and the above-gap anomaly in dV/dI for all the mesoscopic NS hybrid-junction samples used, despite the difference in the junction geometry. This nonlinearity in dV/dI disappears above the transition temperature of the Pb superconducting island. The following observations led to the conclusion that the ZBA is due to the interference of conjugate electron–hole pairs: (i) the excess current I_{exc} exists for all samples and I_{exc} of the overlay junction (Sample OL2) is larger than I_{exc} of the sandwich junction (Sample SW1); (ii) the conductance variation δG qualitatively follows the proximity-effect relation $1/\sqrt{k_B T + eV}$ when $k_B T, eV \gg E_c$; and finally (iii) the ZBA is sensitive to the applied magnetic fields when applied in parallel with the NS interface. We attribute the above-gap anomaly to the local suppression of the superconductivity caused by a high current density through the NS junctions.

Acknowledgements

We wish to acknowledge the useful discussions with Dr. Hekking and Prof. Lambert. One of us (N.K.) appreciates the useful discussions with Dr. Galaktionov, Mr. Cho, and Prof. Ryu. This work was supported by KOSEF, BSRI, MARC, and POSTECH.

References

[1] F.W. Hekking, G. Schön, D.V. Averin (Eds.), Mesoscopic Superconductivity, 203B, Physca, Amsterdam, 1994 (see references therein).
[2] A.F. Andreev, Sov. Phys. JETP 19 (1964) 1228.
[3] G.E. Blonder, M. Tinkham, T.M. Klapwijk, Phys. Rev. B 25 (1982) 4515.
[4] P. Xiong, G. Xiao, R.B. Laibowitz, Phys. Rev. Lett. 71 (1993) 1907.
[5] A. Kastalsky, A.W. Kleinsasser, L.H. Greene, R. Bhat, F.P. Milliken, J.P. Harbison, Phys. Rev. Lett. 67 (1991) 3026.
[6] F.W. Hekking, Yu. Nazarov, Phys. Rev. Lett. 71 (1993) 1625.
[7] F.W. Hekking, Yu. Nazarov, Phys. Rev. B 49 (1994) 6847.
[8] A.F. Volkov, V.V. Pavlovskii, in: C. Giovannella, C.J. Lambert (Eds.), Superconductivity in Networks and Mesoscopic Systems, AIP, New York, 1997.
[9] A.A. Golubov, F.K. Wilhelm, A.D. Zaikin, Phys. Rev. B 55 (1997) 1123.
[10] C.J. Lambert, R. Raimondi, J. Cond. Matt. 10 (1997) 901.
[11] B.J. van Wees, P. de Vries, P. Magnee, T.M. Klapwijk, Phys. Rev. Lett. 69 (1992) 510.
[12] C.W.J. Beenakker, Phys. Rev. B 46 (1992) 12841.
[13] C.W.J. Beenakker, Rev. Mod. Phys. 69 (1997) 731.
[14] I.K. Marmorkos, C.W.J. Beenakker, R.A. Jalabert, Phys. Rev. B 48 (1993) 2811.
[15] H. Pothier, S. Gueron, D. Esteve, M.H. Devoret, Phys. Rev. Lett. 73 (1994) 2488.
[16] V.T. Petrashov, V.N. Antonov, P. Delsing, T. Claeson, Phys. Rev. Lett. 74 (1995) 5268.
[17] P. Charlat, H. Courtois, Ph. Gandit, D. Mailly, A.F. Volkov, B. Pannetier, Phys. Rev. Lett. 77 (1996) 4950.
[18] P. Mohanty, E.M.Q. Jariwala, R.A. Webb, Phys. Rev. Lett. 78 (1997) 3366.
[19] P. Charlat, H. Courtois, B. Pannetier, in: C. Giovannella, C.J. Lambert (Eds.), Superconductivity in Networks and Mesoscopic Systems, AIP, New York, 1997.
[20] C. Nguyen, H. Kroemer, E.L. Hu, Phys. Rev. Lett. 69 (1992) 2847.
[21] M. Tinkham, Introduction to Superconductivity, Krieger, New York, 1980, p. 64.
[22] A.A. Abrikosov, Fundamentals of the Theory of Metals, North-Holland, Amsterdam, 1988, p. 398.